J|A|C|S ARTICLES

Published on Web 02/12/2009

Interfacial Nanostructuring on the Performance of Polymer/ TiO_2 Nanorod Bulk Heterojunction Solar Cells

Yun-Yue Lin,[†] Tsung-Hung Chu,[†] Shao-Sian Li,[†] Chia-Hao Chuang,[†] Chia-Hao Chang,[†] Wei-Fang Su,[†] Ching-Pin Chang,[†,‡] Ming-Wen Chu,[‡] and Chun-Wei Chen*,[†]

Department of Materials Science and Engineering and Center for Condensed Matter Sciences, National Taiwan University, Taipei 106, Taiwan

Received October 19, 2008; E-mail: chunwei@ntu.edu.tw

Abstract: This work presents polymer photovoltaic devices based on poly(3-hexylthiophene) (P3HT) and TiO_2 nanorod hybrid bulk heterojunctions. Interface modification of a TiO_2 nanorod surface is conducted to yield a very promising device performance of 2.20% with a short circuit current density (J_{sc}) of 4.33 mA/cm^2, an open circuit voltage (V_{oc}) of 0.78 V, and a fill factor (FF) of 0.65 under simulated A.M. 1.5 illumination (100 mW/cm^2). The suppression of recombination at P3HT/TiO_2 nanorod interfaces by the attachment of effective ligand molecules substantially improves device performance. The correlation between surface photovoltage and hybrid morphology is revealed by scanning Kelvin probe microscopy. The proposed method provides a new route for fabricating low-cost, environmentally friendly polymer/inorganic hybrid bulk heterojunction photovoltaic devices.

1. Introduction:

Over the past decade, solar cells based on organic dye molecules[1] or conjugated polymers[2−4] have attracted considerable interest because they can be used to fabricate low-cost large-area photovoltaic devices. The most promising device structure of polymer solar cells is based on the bulk heterojunction (BHJ), which consists of an electron-accepting network that is formed randomly within a polymer matrix (donor). Recent advances in the fabrication of poly(3-hexylthiophene)(P3HT)/fullerene derivative bulk heterojunction solar cells have led to efficiencies of 4−5%.[2,4] An alternative type of polymer solar cell, based on a polymer/inorganic nanocrystal hybrid device structure, is also appealing because of relatively high electron mobility and the good physical and chemical stability of inorganic nanocrystals.[5] Various nanocrystals such as CdSe,[3,6] PbS,[7] TiO_2,[8−11] and ZnO[12] have been used in polymer/inorganic nanocrystal hybrid solar cells. Promising power conversion efficiencies from systems based on CdSe nanorods[3] or tetrapods,[6] which comprise enhanced 1D or 3D carrier transport routes, have been achieved by reducing the number of interparticle hopping. Recently, the replacement of such toxic precursors such as Cd or Pb with more environmentally friendly materials, such as metal oxide semiconductors, has also received much interest. The TiO_2 nanocrystal is a candidate for use in hybrid polymer solar cell applications since it is nontoxic and low-cost. The two most popular types of hybrid solar cells based on the polymer/TiO_2 nanocrystals involve the dispersion of nanocrystals in a solution that is blended with a conjugated polymer to form a bulk heterojunction structure[9,11] and the growth of rigid nanoporous or nanorod structures, which can be filled with a polymer to form a nanostructured hybrid solar cell.[8,10] According to most studies on the photovoltaic performance obtained using polymer/TiO_2 hybrids, the power conversion efficiencies are still below 1%. Recently, Goh et al. systematically examined the improvement of photovoltaic performance obtained using the P3HT/TiO_2 bilayer structure through interface modification by the attachment of organic dye molecules to the TiO_2 surface.[13] Nevertheless, the efficiency is still largely limited by the intrinsically small interface area in the bilayer structure. This work will present the photovoltaic performance of poly(3-hexylthiophene)(P3HT)/TiO_2 nanorod hybrid BHJs which consist of many donor/acceptor interfaces for charge separation. Interface modification between a conjugated polymer and TiO_2 nanorods is employed to obtain a very

[†] Department of Materials Science and Engineering.
[‡] Center for Condensed Matter Sciences.

(1) Graetzel, M. *Nature* **2001**, *414*, 338.
(2) Ma, W.; Yang, C.; Gong, X.; Lee, K.; Heeger, A. J. *Adv. Funct. Mater* **2005**, *15*, 1617.
(3) Huynh, W. U.; Dittmer, J. J.; Alivisatos, A. P. *Science* **2002**, *295*, 2425.
(4) Li, G.; Shrotriya, V.; Huang, J.; Yao, Y.; Moriarty, T.; Emery, K.; Yang, Y. *Nat. Mater.* **2005**, *4*, 864.
(5) Bouclé, J; Ravirajan, P; Nelson, J. *J. Mater. Chem.* **2007**, *17*, 3141.
(6) Sun, B.; Snaith, H. J.; Dhoot, A. S.; Westenhoff, S.; Greenham, N. C. *J. Appl. Phys.* **2005**, *97*, 014914.
(7) McDnoald, S. A.; Konstantatos, G.; Zhang, S.; Cyr, P. W.; Klem, E. J. D.; Levina, L.; Sargent, E. H. *Nat. Mater.* **2005**, *4*, 138–142.
(8) Coakley, K. M.; McGehee, M. D. *Appl. Phys. Lett.* **2003**, *83*, 3380–3382.
(9) Chang, C. H.; Huang, T. K.; Lin, Y. T.; Lin, Y. Y.; Chen, C. W.; Chu, T. H.; Su, W. F. *J. Mater. Chem.* **2008**, *18*, 2201–2207.
(10) Ravirajan, P.; Haque, S.A.; Durrant, J. R.; Bradley, D. D. C.; Nelson, J. *Adv. Funct. Mater* **2005**, *15*, 609–618.
(11) (a) Bouclé, J.; Chyla, S; Shaffer, M. S. P; Durrant, J. R.; Bradley, D. D. C.; Nelson, J. *Adv. Funct. Mater.* **2008**, *16*, 622–633. (b) Kwong, C. Y.; Choy, W. C. H.; Djurisic, A. B.; Chui, P. C.; Cheng, K. W.; Chan, W. K. *Nanotechnology* **2004**, *15*, 1156–1161.
(12) Beek, W. J. E.; Wienk, M. M.; Janssen, R. A. J. *Adv. Mater.* **2004**, *16*, 1009–1013.
(13) Goh, C.; Scully, S. R.; McGehee, M. D. *J. Appl. Phys.* **2007**, *101*, 114503.

10.1021/ja8079143 CCC: $40.75

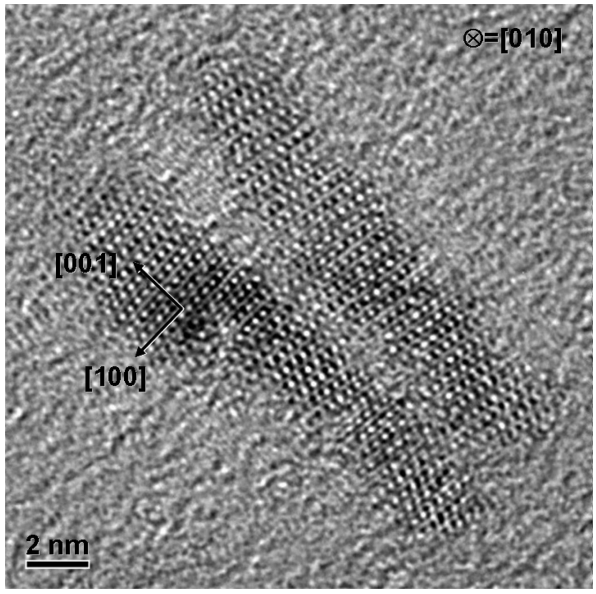

Figure 1. High-resolution TEM (HRTEM) image of TiO_2 nanorods.

promising device performance of 2.20%. The mechanisms by which the carrier dynamics of charge separation, transport, and recombination influence the performance of hybrid solar cells after interface modification will be investigated using time-resolved photoluminescence (TRPL) spectroscopy, time-of-flight (TOF) mobility measurement, and transient open-circuit voltage decay (TOCVD) measurement, respectively. Moreover, the correlation between surface photovoltage and hybrid morphology in (P3HT)/TiO_2 nanorod bulk heterojunctions will be examined, investigated, and visualized using a scanning Kelvin probe microscope (SKPM), supporting the observed enhancement of device performance following interface modification.

2. Experimental Section

2.1. Preparations of Materials. 2.1.1. TiO_2 Nanorods. Anatase TiO_2 nanorods with a high aspect ratio were synthesized as described elsewhere.[14] The dimensions of TiO_2 nanorods were ~20−30 nm in length and 4−5 nm in diameter as shown in the representative high-resolution transmission electron microscopic (HRTEM) image (Figure 1). The experimental contrast of the individual nanorod is characteristic of that of the TiO_2 anatase phase along the [010] zone axis and was homogeneously observed among ~40 nanorods investigated, indicating the purity and homogeneity of the phase achieved using the presented synthesis technique.

2.1.2. Ligand Exchange Processes. The as-synthesized TiO_2 nanorods were capped with an insulating surfactant of oleic acid (O.A.) which comprised a long alkyl chain, which could act as a potential barrier to charge transfer. The surface of the TiO_2 nanorod was therefore modified by ligand exchange treatment, to remove the original O.A. ligand or to replace it with a more effective interfacial molecule. Initially, TiO_2 nanorods were dispersed in pyridine and stirred at 75 °C until the solution turned clear. Accordingly, the original ligand molecules of O.A. were removed, and the pyridine molecules of a weak bonded ligand that were on the surface of the TiO_2 nanorods could be removed by heating. Figure 2 shows the FT-IR spectra in the region 3700−660 cm^{-1} of the TiO_2 nanorod samples before and after pyridine treatment. In the spectra, the bands at 2930 and 2850 cm^{-1} are assigned to the antisymmetric and symmetric C−H stretching vibrations of the

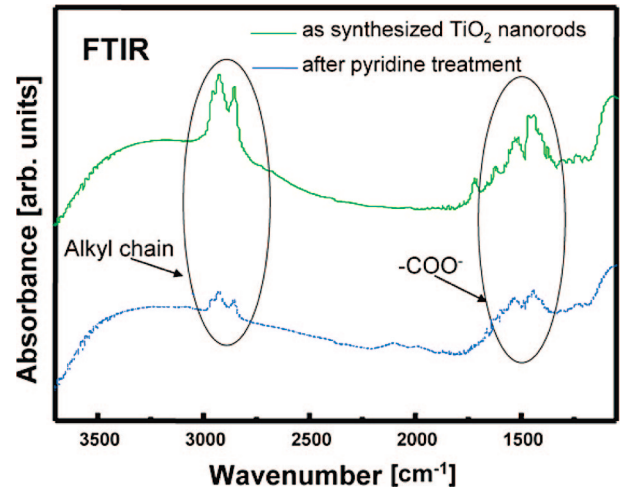

Figure 2. FT-IR spectra of the TiO_2 nanorod samples before and after pyridine treatment.

−CH_2− groups in the hydrocarbon moiety.[15] The shoulder at 2960 cm^{-1} is assigned to the asymmetric stretching of the terminal −CH_3 group of the long alkyl chain.[15] The intense and definite bands centered at 1530 and 1440 cm^{-1}, respectively, are associated with the COO^- antisymmetric and symmetric stretching vibrations of the carboxylate anion complexes with the surface Ti centers.[16] After the insulating surfactant of O.A. has been removed by pyridine treatment, the intensities of the characteristic COO^- bands and the −CH− vibrational bands were much weakened, confirming that the removal of the insulating carboxylic ligands from the surface of the TiO_2 nanorods actually occurred during the process of surface modification.[17] The proportion of residual O.A. following pyridine treatment was ~5 wt % as estimated by thermogravic analysis (TGA, TA Instrument.). The characteristic peaks of pyridine are located at 1581, 1437, 1030, and 991 cm^{-1} and are attributed to the symmetric and asymmetric ring breathing and the C−C and C−N stretching modes, respectively. The amount of pyridine on TiO_2 nanorods was believed to be small because of its ease of removal by heating.[18] Our previous report demonstrated that the removal of insulating ligand on the TiO_2 nanorod surface greatly improves the charge separation efficiency and the fill factor of a device.[9]

Next, three different kinds of ligand molecules of anthracene-9-carboxylic acid (ACA), tetracarboxy phthalocyanine copper (II) (CuPc-dye), and cis-bis(4,4-dicarboxy-2,2-bipyridine)dithiocyanato ruthenium(II)(N3-dye) were then used for interface modification. All of these molecules consist of carboxylate groups −COOH and can be attached strongly to the TiO_2 nanorod surface. Figure 3a schematically depicts a TiO_2 nanorod after interface modification using various interfacial molecules. To obtain the ACA-capped TiO_2 nanorods, ethanol washed bare TiO_2 nanorods were mixed with the ACA in a 6:1 weight ratio and were then dispersed in pyridine, which was stirred at 75 °C until the solution turned clear and yellow. To obtain the CuPc- or N3-dye modified TiO_2 nanorods, the as-synthesized O.A. capped TiO_2 nanorods were mixed with the dyes in an ~500:1 weight ratio, dispersed in pyridine, and left stirring at 75 °C until the solution turned clear and blue (CuPc-dye) and purple (N3-dye). Since the solubility of CuPc- and N3-dye in pyridine is limited, a smaller amount of these molecules can be added during ligand exchange procedures than the amount of ACA. The extraction procedures were subsequently conducted in air. TiO_2

(14) Zeng, T. W.; Lin, Y. Y.; Lo, H. H.; Chen, C. W.; Chen, C. H.; Liou, S. C.; Hunag, H. Y.; Su, W. F. *Nanotechnology* **2006**, *17*, 5387.
(15) Thistlethwaite, P. J.; Hook, M. S. *Langmuir* **2000**, *16*, 4993.
(16) Nara, M.; Torii, H.; Tasumi, M. *J. Phys. Chem.* **1996**, *100*, 19812.
(17) Cozzoli, P. D.; Kornowski, A.; Weller, H. *J. Am. Chem. Soc.* **2003**, *125*, 14539.
(18) Huynh, W. U.; Dittmer, J. J.; Libby, W. C.; Whiting, G. L.; Alivisatos, P. *Adv. Funct. Mater.* **2003**, *13*, 73–79.

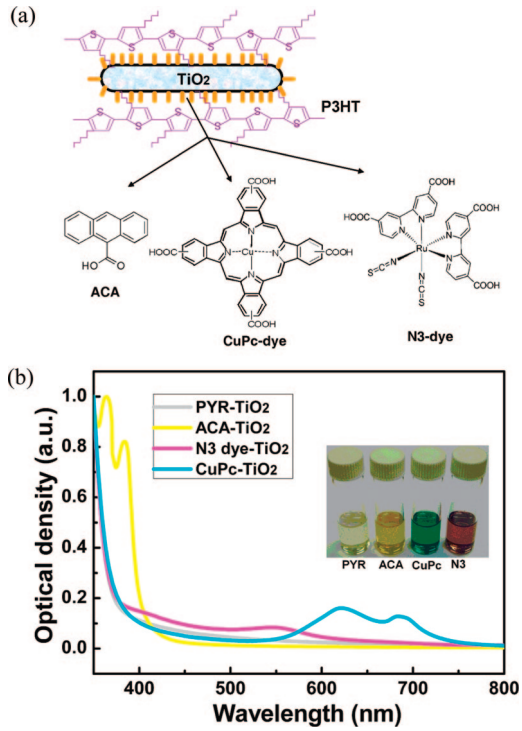

Figure 3. (a) Schematic representations of P3HT/TiO_2 nanorod hybrid after interface modification and chemical structures of different interfacial molecules of ACA, CuPc-dye, and N3-dye molecules respectively. (b) UV−visible absorption spectra of TiO_2 nanorods modified by pyridine treatment and by different interfacial molecules. The inset shows the images of these samples dissolved in solvent.

nanocrystals were readily precipitated upon addition of an excess of hexane to the reaction mixture at room temperature. The resulting precipitates were isolated by centrifugation, and these TiO_2 nanorods modified with interfacial molecules were then redispersed in a mixed solvent which consisted of pyridine, chloroform, and dichloromethane in a 1:2:2 volume ratio, without any further growth or irreversible aggregation. Figure 3b shows the UV−visible absorption spectra of TiO_2 nanorods that have been modified with different interfacial molecules. The typical absorption spectrum of the pyridine-treated TiO_2 nanorods was similar to that of pristine TiO_2 with an edge at ~350 nm. The absorption spectra of ACA, CuPc-dye, and N3-dye modified TiO_2 nanorods from 350 to 400 nm, from 550 to 750 nm, and from 400 to 700 nm correspond to the typical absorption ranges of the respective ligand molecules.[19−21] The amount of dye adsorbed on the TiO_2 nanorods was estimated by comparing the spectroscopic absorbance using the method commonly used in dye-sensitizer solar cells (DSSCs).[22] The size and density of the TiO_2 nanorods were considered to estimate the coverage of the TiO_2 nanorod by dye molecules as shown in Table 1. The hybrid materials were then prepared by adding an appropriate amount of TiO_2 nanorods into P3HT (MW ~60 000, PDI 1.5, RR 96%) polymer solution to make P3HT/TiO_2 nanorod hybrid samples (50:50 wt%) in a mixed solvent, which contained pyridine, chloroform, dichloromethane, and chlorobenzene.

2.2. Device Fabrications. For the photovoltaic device fabrication, a 30 nm-thick layer of PEDOT/PSS (Baytron P 4083) was spin-cast onto the ITO substrate and then baked at 120 °C for 30 min. The highly conductive PEDOT/PSS layer was intended to keep the serial resistance low and to reduce surface roughness. The films were transferred to a nitrogen-purged glovebox for subsequent depositions. A thin active P3HT/TiO_2 nanorod hybrid layer ~150 nm thick was then deposited by using spin coating. An additional thin layer of TiO_2 nanorods, sandwiched between the active layer and the aluminum electrode, was included as a hole blocking layer[14] and also as an optical spacer.[23] The typical device area was ~0.1 cm^2. The Al electrode was then deposited onto the TiO_2 nanorod layer by thermal evaporation in a vacuum at a pressure of ~2×10^{-6} Torr.

Table 1. Amount of Various Dye Molecules Adsorbed on TiO_2 Nanorod Surface

	adsorption amount mol/cm^2 of TiO_2 nanorod
ACA	8.20×10^{-11}
CuPc	1.34×10^{-12}
N3	1.03×10^{-12}

2.3. Material and Device Characterizations. UV−visible absorption spectra were obtained using a Jasco V-570 UV/vis/NIR spectrophotometer. Current−voltage characteristics (Keithley 2410 source meter) were obtained by using a solar simulator (Newport Inc.) with an A.M. 1.5 filter under an irradiation intensity of 100 mW/cm^2. A UV filter with a cutoff of 400 nm was used to avoid the optical excitation of TiO_2. The thickness of the film was measured using a Veeco M6 surface profiler. Time-resolved photoluminescence (TRPL) spectroscopy was performed with a time-correlated single photon counting (TCSPC) spectrometer (Picoquant, Inc.). A pulse laser (470 nm) with an average power of 1 mW operating at 40 MHz with a duration of 70 ps was used for excitation. Measurements of the transient open-circuit voltage decay (TOCVD) of the devices were made under open circuit conditions under illumination of adjustable intensity from a solar simulator. A small perturbation generated by a pulsed laser of a frequency-double Nd:YAG pulsed laser ($\lambda = 532$ nm, repetition rate 10 Hz, duration ~5 ns) is used. The transient decay signals were recorded by a digital oscilloscope (Tetronix TDS5052B). The samples were mounted in a vacuum chamber under 10^{-3} Torr during measurement. Scanning Kelvin probe microscopy (SKPM) was conducted using a MultiModel scanning probe microscope (Digital Instruments, Nanoscope III) under N_2 ambient conditions. A Pt coated cantilever was used to make all measurements, and the resonant frequency of the cantilever was 75 kHz. To make the time-of-flight (TOF) mobility measurement, thick films (>2 μm) were prepared by drop-casting the P3HT/TiO_2 nanorod blended solution onto the substrates. In the electron mobility measurement, a device with a structure of ITO/P3HT/TiO_2 nanorod hybrid/Al was used to extract the signal. In the hole mobility measurement, a semitransparent Al electrode (35 nm) thermally evaporated onto a glass substrate in a vacuum of ~10^{-6} Torr replaced the ITO electrode to form an Al/P3HT/TiO_2 nanorod hybrid/Al device. In the TOF transient photocurrent measurement, a thin layer of charge carriers was generated under illumination through the transparent (or semitransparent) electrodes using a frequency-double Nd:YAG pulsed laser ($\lambda = 532$ nm, repetition rate 10 Hz, duration ~5 ns). Under the applied electric field, these carriers drifted toward the counter electrode, giving the transient photocurrent signal that was recorded by a digital oscilloscope (Tetronix TDS5052B). The carriers (electrons or holes) under study were selected by changing the polarity and magnitude of the applied electric field using a Kiethley 2410 source meter.

3. Results and Discussion

Figure 4a plots the current−voltage characteristics of devices that consisted of various interface-modified TiO_2 nanorods under

(19) Kamat, P. V. *J. Phys. Chem.* **1989**, *93*, 859.
(20) Shen, L.; Zhu, G.; Guo, W.; Tao, C.; Zhang, X.; Liu, C.; Chen, W.; Ruan, S.; Zhong, Z. *Appl. Phys. Lett.* **2008**, *92*, 073307.
(21) Hagfeldt, A.; Grätzel, M. *Acc. Chem. Res.* **2000**, *33*, 269.
(22) Zhang, X.-H.; Li, C.; Wang, W.-B.; Cheng, X.-X.; Wang, X.-S.; Zhang, B.-W. *J. Mater. Chem.* **2007**, *17*, 642–649.
(23) Kim, J. Y.; Kim, S. H.; Lee, H. H.; Lee, K.; Ma, W.; Gong, X.; Heeger, A. J. *Adv. Mater.* **2006**, *18*, 572.

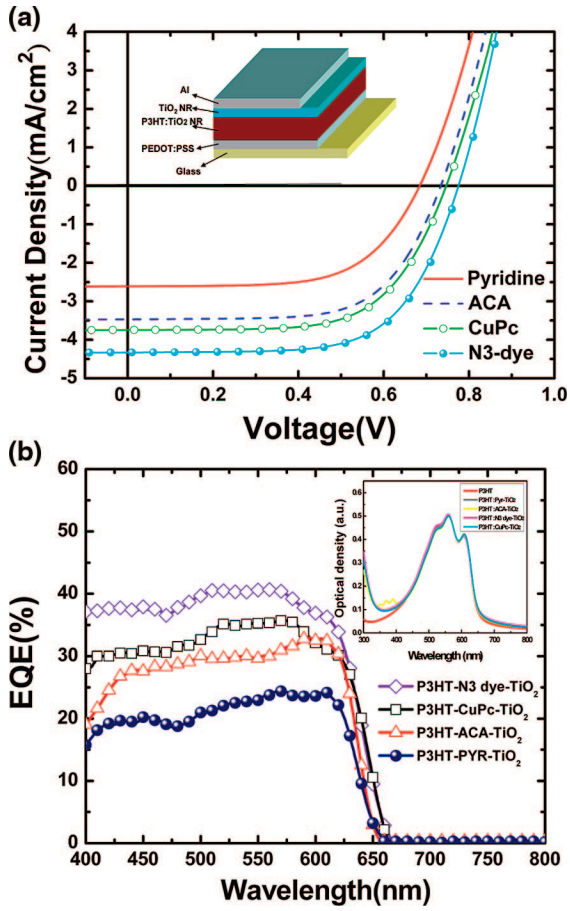

Figure 4. (a) Current−voltage characteristics and (b) external quantum efficiencies (EQEs) of the photovoltaic devices using different interface ligand molecules under A.M. 1.5 (100 mW/cm^2) irradiation. The inset shows the optical density of pristine P3HT and P3HT/TiO_2 nanorod hybrids modified by different interfacial molecules.

Table 2. Device Performance of P3HT/TiO_2 Nanorod BHJ Solar Cells by Pyridine (PYR), ACA, CuPc-dye, and N3-dye modification (under A.M. 1.5, 100 mW/cm^2 irradiation)

	J_{sc} (mA/cm^2)	V_{oc} (V)	FF (%)	η (%)
PYR	2.61	0.69	62	1.12
ACA	3.47	0.74	65	1.67
CuPc	3.74	0.75	64	1.80
N3	4.33	0.78	65	2.20

simulated A.M. 1.5 illumination (100 mW/cm^2). Table 2 presents the overall photovoltaic performance of these devices. After removing the insulating surfactant or replacing with a more effective interface layer on the TiO_2 nanorod surface, all of the devices had fill factors (FF) from 0.62 to 0.65 which are relatively high for the organic solar cells. The result indicates that the serial and shunt resistance of the devices can be largely improved through interface modification. Additionally, both the short circuit current (J_{sc}) and the open circuit voltage (V_{oc}) can also be improved by interfacial engineering between P3HT and TiO_2 nanorods, suggesting that the interface layer may crucially determine the device performance of the P3HT/TiO_2 nanorod bulk heterojunctions. Among these devices, the solar cell that comprises TiO_2 nanorods modified by the N3-dye molecule demonstrates the best device performance with a J_{sc} of 4.33 mA/cm^2, a V_{oc} of 0.78 V, and an FF of 0.65, yielding a power conversion efficiency (η) of 2.20%, which is the highest reported

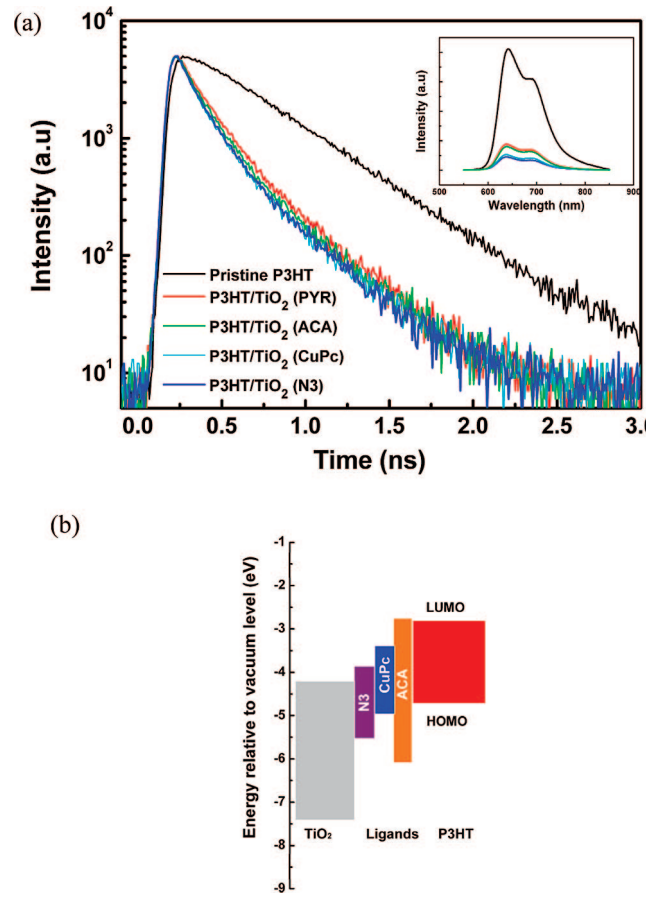

Figure 5. (a) TRPL spectroscopy of P3HT/TiO_2 nanorod hybrids following different interface modifications. The decay time for the pristine P3HT is 680 ps. The inset shows the PL intensities of these samples. (b) The corresponding energy levels of various materials.

efficiency for the polymer/TiO_2 hybrid solar cells. Figure 4b shows the corresponding external quantum efficiency (EQE) of these devices based on P3HT/TiO_2 nanorod hybrids after interface modification. EQE spectra with a similar shape are obtained from these devices, with no contribution beyond the absorption edge of P3HT, consistent with the negligible optical density of interface layers of these molecules in relation to that of P3HT (inset). This result indicates that these ligand molecules modify the interface rather than harvest light.

The interfacial molecules can (i) facilitate charge separation or (ii) prevent back recombination at the interfaces of P3HT/TiO_2 nanorod hybrids. Time-resolved photoluminescence spectroscopy (TRPL) and transient open-circuit voltage decay (TOCVD) measurements were performed to examine the two types of carrier dynamics in hybrids after interface modification. Figure 5a shows the TRPL decay curves of the pristine P3HT and the P3HT/TiO_2 nanorod hybrid films through interface modification. All P3HT/TiO_2 nanorod hybrid samples demonstrate efficient charge transfer at interfaces after the insulating surfactant has been removed or replaced with a more effective interface layer, by showing a shorter PL lifetime τ than that of the pristine P3HT. The inset shows the corresponding PL quench efficiency of the hybrids. The PL quenching rates of P3HT/TiO_2 nanorod hybrids by pyridine, ACA, CuPc-dye, and N3-dye modifications as percentages of that of pristine P3HT are 78.1%, 81.8%, 87.4%, and 89%. The measured PL lifetime τ of the pristine P3HT and P3HT/TiO_2 nanorod hybrids following modifications with pyridine, ACA, CuPc-dye, and N3-dye are τ_{P3HT} = 680 ps, τ_{PYR} = 255 ps, τ_{ACA} = 246 ps, τ_{CuPc} =

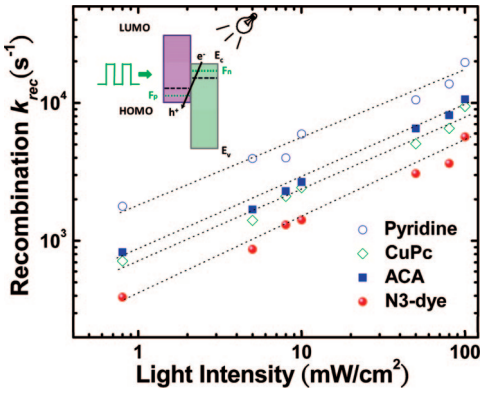

Figure 6. Charge recombination rate constant k_{rec} versus light intensity at V_{oc} determined by TOCVD measurement. The inset schematically depicts the recombination mechanism and TOCVD setup.

235 ps, and $\tau_{N3} = 232$ ps, respectively. The improved charge separation at the P3HT/TiO_2 nanorod interfaces may be attributed to the following reasons. First, the attachment of effective interfacial molecules on the surface of TiO_2 nanorods may improve the compatibility between the polymer and TiO_2 nanorods, where the π-conjugated structures in the interfacial molecules can interact with the thiophene rings of P3HT (see Supporting Information Figure S1). The improved compatibility of the morphology of hybrids can result in a more effective diffusion of excitons to the appropriate TiO_2 nanorod surface sites but not along the side chains of the polymer, which could inhibit the diffusion of excitons to interfaces for charge separation. The interface modifiers attached by chemical bonding next to TiO_2 nanorods (ACA, CuPc-dye, and N3-dye modified samples) can lead to more efficient electronic coupling between the polymer and TiO_2 nanorods. Additionally, the interface modifiers of CuPc or N3-dye molecules can mediate charge transfer between the polymer and TiO_2 nanorods more effectively than the ACA molecule because the ACA molecule has a higher LUMO energy level than CuPc- and N3-dye molecules. Figure 5b presents the corresponding energy levels of different materials taken from the literature.[19−21] Interface modifiers are also believed to be able to modify the surface traps or defects of TiO_2 nanorods.

However, the effect of enhanced charge separation efficiency alone can not account for the significant improvement in both J_{sc} and V_{oc} of devices upon interface modification. Accordingly, transient open-circuit voltage decay (TOCVD) measurements were performed to determine the recombination rate at the interfaces between polymer and TiO_2 nanorods in an operating solar cell device under a V_{oc} condition. If no charge is being collected under the open-circuit condition, then the voltage that is generated in the solar cell is considered to be the difference between the quasi-Fermi level (E_{fn}) of electrons in TiO_2 nanorods and the quasi-Fermi level (E_{fp}) of holes in P3HT. A small perturbation generated by a pulsed laser produces extra electrons and holes in hybrids. The decay of the photovoltage that is generated by the additional carriers due to the small perturbation corresponds to the recombination rate at the heterojunctions. Figure 6 plots the charge recombination rate constant k_{rec} versus illumination intensity under open circuit conditions. The recombination rates k_{rec} follow the order pyridine-modified sample → ACA → CuPc-dye → N3-dye modified samples at all light intensities, showing good consistency with the photovoltaic performance. The interface modifier of the N3-dye molecule acts as the most effective recombination barrier with respect to other ligand molecules. As described above, the reduced recombination rate may lead to increased electron and hole concentrations at interfaces, increasing the difference between the quasi-Fermi levels of electrons and holes, and accounting for the observed increase in V_{oc} upon interface modifications. Furthermore, the suppression of back recombination at the interfaces can increase the number of carriers that can be transported toward electrodes, as a result of improved J_{sc} after interface modification. The increase in both J_{sc} and V_{oc} with a reduced recombination rate also shows excellent agreement with the theoretical model that was presented by Ferber et al.[24]

To further investigate the correlation between morphology associated with interface recombination of the hybrids and various interface modifiers, noncontact scanning Kelvin probe microscopy (SKPM) was employed to measure the photoinduced surface photovoltage with a lateral resolution of less than 100 nm and a potential resolution of ~10 mV.[25] SKPM enables simultaneous measurement of the morphology and the electronic properties of a surface and has been found to be very useful in investigating the mechanism of charge injection, transport, and trapping in organic transistors.[26] Recently, several groups have utilized SKPM to probe the surface potential maps of polymer/polymer[27,28] and polymer/fullerene[29] hybrid solar cells under photoexcitation. Figure 7a shows the atomic force microscope (AFM) topographic image of the P3HT/TiO_2 nanorod (N3-dye modified) hybrid spin cast on an oxygen-plasma-cleaned ITO-coated glass substrate. Figure 7b and c show the corresponding surface potential measured in the dark and under illumination, respectively. When the device is illuminated, the photogenerated excitons are dissociated at the polymer/TiO_2 nanorod interfaces, where holes diffuse toward the ITO anode through the P3HT regions, while electrons diffuse toward the surface through the TiO_2 nanorod regions. Consequently, a large image contrast in the local work function map of the N3-modified hybrid sample under illumination is observed (Figure 7c). The negative shift in the work function in all regions under illumination is caused by an accumulation of negatively charged carriers on the surface.[29] The darker region, where the work function is lower, corresponds to the TiO_2-nanorod-rich phase, where more electrons are accumulated on the surface. In contrast, the brighter region corresponds to the P3HT-rich phase with a higher value of work function. The interpenetration of two macrophases through the film to the substrate has been observed, suggesting the formation of bicontinuous pathways for electron and hole transport in an efficient bulk heterojunction solar cell. In each macrophase region, TiO_2 nanorods (P3HT) are clearly observed embedded within the P3HT-rich (TiO_2 nanorod-rich) macrophase region. Notably, the finer scale of phase separation which is responsible for charge separation at P3HT/TiO_2 nanorod interfaces is beyond the resolution limit of our experimental setup because of the short exciton diffusion

(24) Ferber, J.; Stangl, R.; Luther, J. *Sol. Energy Mater. Sol. Cells* **1998**, *53*, 29.
(25) Palermo, V.; Palma, M.; Samorì, P. *Adv. Mater.* **2006**, *18*, 145.
(26) Bürgi, L.; Richards, T. J.; Friend, R. H.; Sirringhaus, H. *J. Appl. Phys.* **2003**, *94*, 6129.
(27) Chiesa, M.; Bürgi, L.; Kim, J. S.; Shikler, R.; Friend, R. H.; Sirringhaus, H. *Nano Lett.* **2005**, *5*, 559.
(28) Coffey, D. C.; Ginger, D. S. *Nat. Mater.* **2006**, *5*, 735.
(29) (a) Hoppe, H.; Glatzel, T.; Niggemann, M.; Hinsch, A.; Lux-Steiner, M. Ch.; Sariciftci, N. S. *Nano Lett.* **2005**, *5*, 269–274. (b) Glatzel, T.; Hoppe, H.; Sariciftci, N. S.; Lux-Steiner, M. Ch.; Komiyama, M. *Jpn. J. Appl. Phys.* **2005**, *44*, 5370.

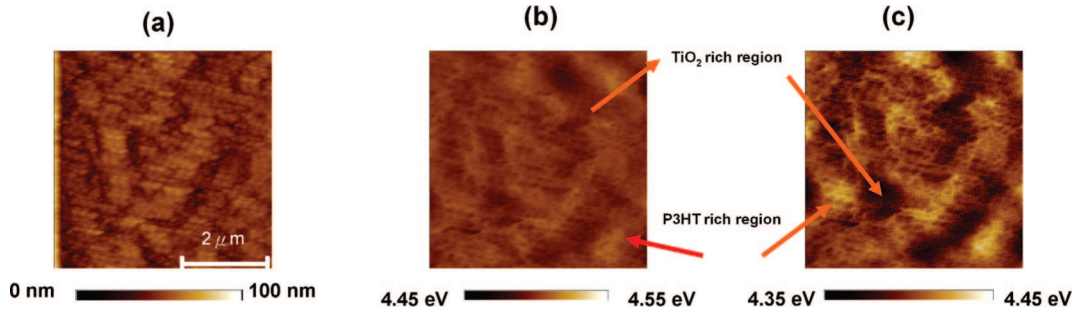

Figure 7. Topography (a) and work function mapping images of N3-modified P3HT/TiO_2 nanorod hybrid sample (b) in the dark (c) under illumination by white light (tungsten halogen lamp, 40 mW/cm^2).

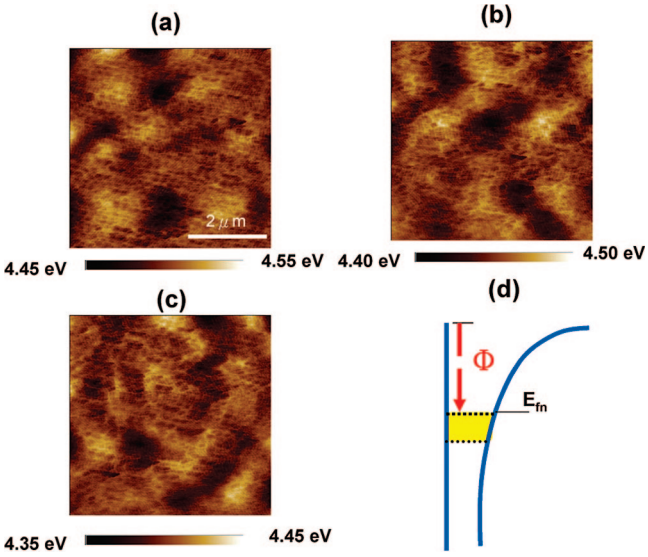

Figure 8. (a−c) Local work function mapping images of polymer/TiO_2 nanorod hybrid films consisting of ACA, CuPc-dye, and N3-dye interface molecules under illumination. (d) Schematic representation of charge accumulation on surface of films under illumination.

length of the polymer (<20 nm).[30,31] Figure 8a−c show the local work function mapping images of polymer/TiO_2 nanorod hybrid films consisting of different interfacial molecules under illumination. Figure 8d schematically depicts the change in the quasi-Fermi level (E_{fn}) for electrons and the local work function Φ of TiO_2 induced by illumination. The mean work function follows the order ACA → CuPc → N3-dye modified samples, indicating that the electrons now can inject into the Al electrode more effectively in the N3-dye modified sample than in the CuPc-dye or ACA-modified samples. This result is consistent with the fact that the N3-modified sample has the slowest recombination rate associated with the best device performance. To further explain the variation in the recombination rate at the polymer/TiO_2 nanorod interfaces modified with different interfacial molecules, the optimized molecular structures of ACA, CuPc-dye, and N3-dye molecules were obtained using the first-principles calculations (see Supporting Information Figure S2). The ACA and CuPc-dye molecules have a planar structure with typical π-conjugated characters of sp^2 hybridization. The size of the CuPc-dye molecule is much larger than that of the ACA molecule, which can act as a more effective barrier to back recombination. Although the coverage of the TiO_2 nanorod surface by ACA molecules markedly exceeds that by the N3-dye molecule as seen in Table 1, the N3-dye molecule is more bulky and less planar, slowing down the recombination kinetics more effectively. A recent report of the dye sensitizer solar cell also demonstrated that the planar organic dye may not be as effective as a bulky N719 counterpart when used as a recombination barrier.[32] The above result suggests that the large improvement in device performance obtained using the N3-modified sample is mainly attributed to the strong suppression of back recombination at interfaces. Finally, the electron and hole mobilities of hybrid materials after interface modification were measured by the TOF technique. The electron and hole mobilities did not vary significantly among these samples (see Supporting Information Figure 3). All of these samples exhibit mobility values in the range $(1.0-2.0) \times 10^{-3}$ $cm^2/V \cdot s$ with very balanced electron and hole transport characteristics, which favor solar cell applications.

4. Conclusion

This work demonstrated the feasibility of solution-processable, low-cost, and environmentally friendly polymer/TiO_2 nanorod bulk heterojunction photovoltaic devices. Interface modifications on the TiO_2 nanorod surface were used to improve the device performance significantly by enhancing charge separation, improving compatibility, and strongly suppressing back recombination. A 3D and bulky interface molecule slows down the recombination more effectively than a planar molecule. The device performance can be improved further by optimizing the size of the TiO_2 nanorods, improving their crystalline quality, or aligning them to improve carrier transport.

Acknowledgment. This work is supported by the National Science Council, Taiwan (Project No. NSC 96-2112-M-002-030-MY3 and 95-3114-P-002-003-MY3).

Note Added after ASAP Publication. After this paper was published ASAP February 12, 2009, the FF value for N3 was corrected in Table 2. The corrected version was published February 25, 2009.

Supporting Information Available: Detailed information on atomic force microscopy (AFM) morphology, optimized molecular structure by first-principles calculations and time-of-flight (TOF) mobility measurements. This information is available free of charge via the Internet at http://pubs.acs.org.

JA8079143

(30) Friend, R. H.; Denton, G. J.; Halls, J. J. M.; Harrison, N. T.; Holmes, A. B.; Kohler, A.; Lux, A.; Moratti, S. C.; Pichler, K.; Tessler, N.; Towns, K.; Wittmann, H. F. *Solid State Commun.* **1997**, *102*, 249.
(31) Savenije, T. J.; Warman, J. M.; Goossens, A. *Chem. Phys. Lett.* **1998**, *287*, 148.
(32) Burke, A.; Ito, S.; Snaith, H.; Bach, U.; Kwiatkowski, J.; Grätzel, M. *Nano Lett.* **2008**, *8*, 977.